2nd IFAC Workshop on Automatic Control in Offshore Oil and Gas Production,
May 27-29, 2015, Florianópolis, Brazil

Model-based drilling fluid flow rate estimation using Venturi flume

C. Berg [*] **A. Malagalage** [**] **C. E. Agu** [***] **G.-O. Kaasa** [*]
K. Vaagsaether [***] **B. Lie** [***]

[*] *Kelda Drilling Controls AS, Porsgrunn, Norway*
[**] *Tel-Tek, Porsgrunn, Norway*
[***] *Telemark University College, Porsgrunn, Norway, (e-mail: Bernt.Lie@hit.no)*

Abstract: Monitoring the flow rate out of the well is critical for good control of the downhole pressure in drilling operations. In this feasibility study, we explore the possibility of using a Venturi flume to provide a cost-effective measurement of the flow rate, with improved accuracy compared to conventional methods. A Venturi flume has been simulated both using CFD and a simplified 1D model. By proper design of the Venturi flume, a jump in the fluid level in the throat section of the flume can be injected. Four methods of using this jump information are discussed, each with their own advantages and disadvantages, such as dependence on fluid properties, length of the flume, computation time, etc. Further work is necessary to improve sensor set-up and numeric methods, as well as testing out the concepts on a Venturi rig.

Keywords: Flow measurement, Models, Partial differential equations, Model approximation, Estimators

1. INTRODUCTION

1.1 Background

Control of the downhole pressure is critical in drilling operations. If the downhole pressure exceeds the strength of the formation, the wellbore might be fractured, causing a loss of drilling fluid to the formation and possibly damaging the reservoir. In the worst case, such a damage may cause an uncontrolled reduction in the downhole pressure. If, on the other hand, the downhole pressure reduces below the formation pore pressure, this may cause an unwanted influx of formation fluid into the wellbore and up the annulus, referred to as a kick, which in the worst case could escalate to a blow-out of hydrocarbons on the rig, e.g. the Deepwater Horizon incident, Hauge and Øien (2012). For safe operation, the downhole pressure should thus be kept within a window defined by the formation fracture pressure and the formation pore pressure.

Early detection of loss of drilling fluid to the formation or of a kick is the most effective measure that can be taken to eliminate or limit the consequences of such incidents. A prerequisite for detecting loss to the formation or kick during drilling operations is monitoring of the mass balance of the well, i.e. the flow of drilling fluid out of the well compared to that pumped into the well.

In conventional drilling, the flow rate out of the well is typically measured by a paddle in the open channel running to the mud pits on the rig. This is an inaccurate measurement that limits the resolution of kick/loss detection. A possible alternative is to use a Venturi flume: an open flume with a constriction, and designed to give a jump in the fluid level which holds information about the flow rate. Venturi flumes are typically used to measure large flows of water, and are rarely used in oil drilling. For drilling fluid flow, particle settling is not desired; Venturi flumes have no dead zone, and are thus suitable.

An important concept in fluid flow is that of critical flow. Consider throwing a pebble in a running fluid flow, with resulting ripples spreading in all directions at the wave velocity of the fluid. If the fluid velocity equals the wave velocity, the ripples spreading in the direction opposite to the flow are stagnant wrt. to a frame fixed to the ground; the flow is critical. If the fluid flow is larger than the wave velocity, the flow is supercritical, while if the fluid flow is smaller than the wave velocity, the flow is subcritical.

1.2 Previous work

The Venturi measurement principle is described in introductory books on fluid mechanics. The use of Venturi flume for measurement in hydrology is described e.g. in Gupta (2008). For use in oil rigs, it is necessary to consider variations in viscosity, the presence of rock chips, etc. Thus a more detailed study is called for.

A flume used for the transport and flow measurement should be designed for so-called supercritical flow conditions, Wilson (1991), Smith et al. (1981). A current flume design based on ISO 4359 standard is applied to so-called subcritical upstream conditions, ISO (2013). There has been some research on the requirements for supercritical flume design. A procedure for designing and using a supercritical flume where it is assumed that so-called critical flow conditions occur at the entrance of the channel throat is outlined in Smith et al. (1981). Little information is

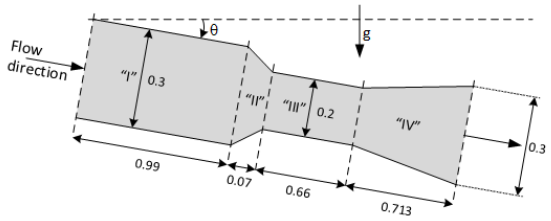

Fig. 1. Geometry of Venturi flume as seen from above: all measures are in [m]. Note that the section lengths are not to scale. Sections "I" and "III" have constant width. g is gravity and θ is the slope angle.

available on flow with non-Newtonian fluids such as used in drilling.

1.3 Structure of paper

In this work, we explore the possibility of using a Venturi flume to provide a cost-effective measurement of the flow rate out of the well, with improved accuracy compared to the flow paddle. In order to compare simulation results with those published in the literature, the experimental set-up of Smith et al. (1981) is used.

In Section 2, the experimental set-up is discussed. In Section 3, models for detailed 3D CFD analysis is discussed, as well as for a simplified 1D approximation. In Section 4, simulation results are presented, and the results are discussed. Some conclusions are drawn in Section 5.

The contributions of the paper are in comparing Venturi flume models using Computational Fluid Dynamics (CFD) for Newtonian fluids to published experimental results, then use CFD for non-Newtonian fluids, comparing CFD models with simplified 1D dynamic models and steady state models. The question is thus: can a Venturi flume be used to estimate relevant information for use in the drilling operation, and how complex a model is needed?

2. EXPERIMENTAL SET-UP

Consider a Venturi flume as seen from above in Fig. 1, with 5 sections numbered "I" through "V".

The slope angle θ of the flume bed can be changed.

With slope angle $\theta = 0$, this Venturi flume appears in the literature [1] as a test case for CFD solvers, using water as fluid and allowing a volumetric flow rate of $[2, 250]$ [m3/h]. In this paper, this nominal flume is used for comparing 3D simulation of water with the results from the literature, as well as with results from a simplified 1D simulation. Furthermore, we use the flume with slope angle $\theta = 4°$ and drilling fluid to study the flow with approximate 1D simulations, and discuss modifications of the flume to make it more suitable for flow measurements of drilling fluid.

3. MODELS OF VENTURI FLUME

3.1 CFD model

Navier Stokes equations For 3D simulations, CFD [2] relies on solving the Navier Stokes equations. These can be stated as (1) for conservation of mass and (2) for conservation of momentum for a Newtonian fluid, Versteeg and Malalasekera (2007)

$$\frac{\partial \rho}{\partial t} + \nabla \cdot (\rho v) = 0 \tag{1}$$

$$\frac{\partial}{\partial t}(\rho v_\varsigma) + \nabla \cdot (\rho v_\varsigma v) = -\frac{\partial p}{\partial \varsigma} + \nabla \cdot (\mu \nabla (v_\varsigma)) + s_\varsigma \tag{2}$$

In (2), ρ is density and $v \in \mathbb{R}^3$ is the velocity vector with components v_ς where $\varsigma \in \{x, y, z\}$. p is pressure and $s \in \mathbb{R}^3$ with components s_ς is additional momentum source terms such as gravity. Modelling non-Newtonian fluids require a different closure to the shear stresses. For incompressible flows (1) reduces to $\nabla \cdot (v) = 0$.

Shear stress For Newtonian fluids, stress τ is proportional to strain rate $\gamma_{\vartheta\varsigma} = \frac{\partial v_\vartheta}{\partial \varsigma}$, and the stress tensor is $\tau = \mu\gamma$ where viscosity μ is very sensitive to temperature. For the Newtonian base case simulations, the fluid is defined as water at 20° [C]. For the non-Newtonian simulations, the *Herschel-Bulkley* model is used, ANSYS-Inc (2011)

$$\tau = \tau_0 + K\gamma^{\frac{1}{\epsilon}} \tag{3}$$

where τ_0 is the excess shear stress, K is the flow behavior index, and $\frac{1}{\epsilon}$ is the fluid consistency index. Here τ_0, K and ϵ are rheological fitting parameters that can be determined by experiments.

Open channel description To track the interface in an open channel problem, the volume of fluid method (VOF) is commonly used, Hirt and Nichols (1981). In VOF an additional variable χ is introduced to represent the volume fraction of a phase in the discretized cell; $\chi = 1$ implies a cell completely filled with the fluid, $\chi = 0$ implies a cell void of the fluid, while $\chi \in (0, 1)$ implies that the cell contains the fluid surface. χ is given by (4),

$$\frac{\partial \chi}{\partial t} + v \cdot \nabla (\chi) = 0 \tag{4}$$

There are different ways to solve this equation; the normal finite volume schemes do not capture the discontinuous nature of χ at the interface. The High Resolution Interface Capture (HRIC) scheme, ANSYS-Inc (2011), is used in this work, and is an implicit finite volume method (FVM) designed to solve this type of interface equation while not being overly diffusive.

Turbulence and discretization Turbulence is in principle included in the above model, but requires infinitely fine discretization in time and space to be accurate. In practice, turbulence is instead introduced by doing time averaging of (2), by introducing "turbulent viscosity", and by introducing turbulent kinetic energy and its diffusion and relation to turbulent viscosity. In this work the common Reynolds Averaged Navier Stokes (RANS) $k - \epsilon$ model is used, Versteeg and Malalasekera (2007).

For discretization of (2) and the two extra turbulence quantities, both the first order upwind and second order upwind schemes are used. For pressure velocity coupling

[1] www.bamo.eu/international/_ftp/msa755-14.pdf
[2] CFD = Computational Fluid Dynamics

both the SIMPLE (Semi Implicit Method For Pressure Linked Equations), ANSYS-Inc (2011), and PISO (Pressure Implicit with Splitting of Operators), ANSYS-Inc (2011), are used.

Boundary and initial conditions The inlet boundary conditions are specified as a mass flow inlet (Section "I") with a specified free surface level and mass flows of liquid and gas (air) specified individually. The lightest phase (gas) is specified as the primary phase. The outlet conditions are specified as a pressure outlet, with the pressure profile set to "from neighboring cell" as the fluid is expected to have supercritical flow ((11), etc.) at the outlet. All walls are specified as no-slip walls, and the default $k-\epsilon$ ANSYS-Fluent wall function is used, ANSYS-Inc (2011). The top of the channel is specified as a pressure outlet with atmospheric pressure. To save computational time, the symmetry of the flume is exploited.

For initialization of the problem both patching the fluid volume with a flat liquid level and running the simulations starting with a "empty" channel is used.

Solver settings and meshing All simulations used the staggered grid, finite volume CFD solver ANSYS-Fluent. The simulations are run in transient using the first order implicit formulation until a steady state solution is obtained. Assessing convergence can be a challenge in CFD, and the residuals may not provide the full picture, Versteeg and Malalasekera (2007). Therefore in addition to monitoring the residuals, multiple surface monitors monitoring the weighted average velocity perpendicular to the flow direction are used to assess convergence. When the simulations are deemed to be in steady state, the solver is switched to steady state and all residuals are reduced to 10^{-4}.

For all 3D drawing and meshing the CFD pre-processor GAMBIT is used. A structured mesh is used, leading to a cell count for the mesh (half geometry) of ca. 3×10^5. Symmetry along the x axis is utilized.

3.2 Approximate 1D model

The Saint Venant Equations Under certain assumptions including uniform flow in cross sectional area A in the x-direction, the Navier Stokes equations can be simplified to the Saint Venant Equations (SVE), Aldrighetti (2007), (5)–(6)

$$\frac{\partial A}{\partial t} = -\frac{\partial \dot{V}}{\partial x} \tag{5}$$

$$\frac{\partial \dot{V}}{\partial t} = -\frac{\partial}{\partial x}\left(\frac{\dot{V}^2}{A}\right) - gA\frac{\partial h}{\partial x}\cos\theta + gA\sin\theta - \frac{F'_{\mathrm{f}}}{\rho} \tag{6}$$

where $\dot{V}$ is volumetric flow rate, g is gravity, h is fluid surface level, and F'_{f} is the friction force per unit length. Level h and cross sectional area A are related via the geometry of the flume. For these types of equations, a *friction slope* S_{f} is introduced, related to F'_{f} as

$$\frac{F'_{\mathrm{f}}}{\rho} \triangleq gAS_{\mathrm{f}}.$$

For filled pipes, the friction slope would be

$$S_{\mathrm{f}} = \frac{f}{2}\frac{\frac{\dot{V}}{A}\left|\frac{\dot{V}}{A}\right|\wp}{gA} \tag{7}$$

where $\wp$ is the wetting perimeter and f is Fanning's friction factor Bird et al. (2002). For shallow water in open flumes, the Gauckler–Manning–Strickler formula is often used, Chow (1959)

$$S_{\mathrm{f}} = k_{\mathrm{M}}^2\frac{\frac{\dot{V}}{A}\left|\frac{\dot{V}}{A}\right|\wp^{4/3}}{A^{4/3}}, \tag{8}$$

where k_{M} is Manning's friction coefficient.

In Jin and Fread (1997), an approximate friction slope for the Herschel-Bulkley model in (3) is given as

$$S_{\mathrm{f}} = \frac{\tau_0}{\rho g\frac{A}{\wp}}\left[1 + \left(\frac{(\epsilon+1)(\epsilon+2)\left|\frac{\dot{V}}{A}\right|}{(0.74+0.656\epsilon)\left(\frac{\tau_0}{K}\right)^{\epsilon}\frac{A}{\wp}}\right)\right]^{\frac{1}{\epsilon+0.15}}. \tag{9}$$

Wave velocities By linearizing the SVE around the steady solution (subscript s), the model can be decomposed into two advection equations of form Martinson and Barton (2002)

$$\frac{\partial \sigma_j}{\partial t} = -\lambda_j\frac{\partial \sigma_j}{\partial x} + \phi_j$$

where the wave velocities λ_j are given by

$$\lambda = \left(\sqrt{\frac{gA_{\mathrm{s}}\cos\theta}{\frac{\partial A}{\partial h}\big|_{\mathrm{s}}}}\cdot(N_{\mathrm{Fr}}+1),\ \sqrt{\frac{gA_{\mathrm{s}}\cos\theta}{\frac{\partial A}{\partial h}\big|_{\mathrm{s}}}}\cdot(N_{\mathrm{Fr}}-1)\right), \tag{10}$$

and the *Froude number* N_{Fr} is given as

$$N_{\mathrm{Fr}} \triangleq \frac{\frac{\dot{V}_{\mathrm{s}}}{A_{\mathrm{s}}}}{\sqrt{\frac{gA_{\mathrm{s}}\cos\theta}{\frac{\partial A}{\partial h}\big|_{\mathrm{s}}}}}. \tag{11}$$

For high velocity flow, $N_{\mathrm{Fr}} > 1$ (*supercritical* flow), both wave velocities are positive, and both boundary conditions $(h,\ \dot{V})$ must be given at $x = 0$. For low velocity flow, $N_{\mathrm{Fr}} < 1$ (*subcritical* flow), one wave velocity is positive, and the other is negative, and one boundary condition must be given at $x = 0$ while the other must be given at $x = L$.

Steady state analysis In this section, subindex "s" is introduced to indicate steady operation. In steady state, $\dot{V}_{\mathrm{s}}$ is constant, and the remaining equation can be rewritten as

$$\frac{dh_{\mathrm{s}}}{dx} = \frac{\frac{\dot{V}_{\mathrm{s}}^2}{gA_{\mathrm{s}}^3}\frac{\Delta W}{L_{\mathrm{r}}}h_{\mathrm{s}} + (\sin\theta - S_{\mathrm{fs}})}{\cos\theta\,(1-N_{\mathrm{Fr}}^2)} \tag{12}$$

where it has been assumed that area A forms an isosceles trapezoid with change of width ΔW over length L_{r} of the flume reach. Comparing with Fig. 1, $L_{\mathrm{r}} = 0.99$ for Section "I"; $\Delta W = 0.3-0.2 = 0.1$ for Section "II", etc. The *critical condition* occurs when $N_{\mathrm{Fr}} = 1$, which leads to the critical level $h_{\mathrm{s}}^{\mathrm{c}}$ given by

$$A^3\left(h_{\mathrm{s}}^{\mathrm{c}}\right) = \frac{\dot{V}_{\mathrm{s}}^2}{g\cos\theta}\left.\frac{\partial A}{\partial h}\right|_{\mathrm{s}}^{\mathrm{c}}. \tag{13}$$

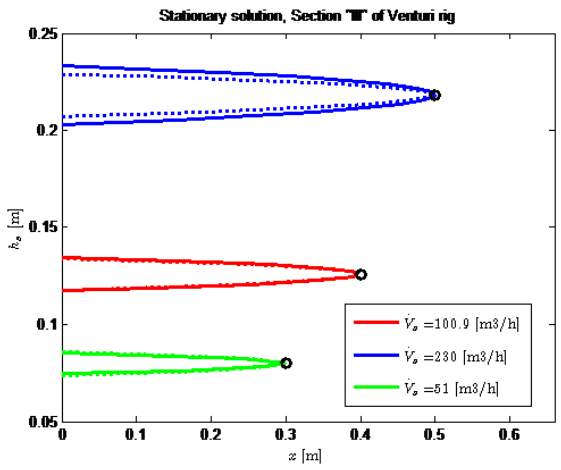

Fig. 2. Analytic solution $h_{\mathrm{s}}(x)$ for Section "III" of Fig. 1 with specified critical point $(x_{\mathrm{c}}, h_{\mathrm{s}}^{\mathrm{c}})$ (black circle), assuming Fanning friction with $f = 0.002$ (solid) and assuming Manning friction with $W \gg h_{\mathrm{s}}$ (dotted).

At the critical condition (level $h_{\mathrm{s}}^{\mathrm{c}}$, at position x_{c}), the model in (12) breaks down.

With $\Delta W = 0$ and rectangular A with flume width W, the critical level from (13) becomes

$$h_{\mathrm{s}}^{\mathrm{c}} = \left(\frac{\dot{V}_{\mathrm{s}}^2}{gW^2 \cos\theta} \right)^{\frac{1}{3}} \tag{14}$$

For this case of $\Delta W = 0$ and flume width W, supercritical flow implies $h_{\mathrm{s}} < h_{\mathrm{s}}^{\mathrm{c}}$, while subcritical flow implies $h_{\mathrm{s}} > h_{\mathrm{s}}^{\mathrm{c}}$.

The *uniform* level is found as $\frac{dh_{\mathrm{s}}}{dx} = 0 \Longrightarrow S_{\mathrm{fs}} = \sin\theta \geq 0$. With $\Delta W = 0$ and flume width W, the wetting perimeter is $\wp = W + 2h$. For Manning friction, the uniform level is thus found by solving the implicit equation

$$k_{\mathrm{M}}^2 \frac{\frac{\dot{V}_{\mathrm{s}}}{h_{\mathrm{s}}^{\mathrm{u}} W} \left| \frac{\dot{V}_{\mathrm{s}}}{h_{\mathrm{s}}^{\mathrm{u}} W} \right| (W + 2h_{\mathrm{s}}^{\mathrm{u}})^{4/3}}{(h_{\mathrm{s}}^{\mathrm{u}} W)^{4/3}} = \sin\theta; \tag{15}$$

we see that this expression breaks down when $\theta = 0$.

With $\Delta W = 0$, (12) is a separable differential equation, and analytic solutions can be found in some cases, giving implicit expressions for h_{s} in the form $x = \mathcal{F}(h_{\mathrm{s}})$. By computing a number of values x for h_{s} in a given range while requiring that the *solution goes through the critical point* denoted $(x_{\mathrm{c}}, h_{\mathrm{s}}^{\mathrm{c}})$, typical solutions are as in Fig. 2.

A key point here is that the steady model in (12) with $\theta = 0$ does not admit a solution for $x > x_{\mathrm{c}}$when the solution is required to go through the critical point. Obviously, the system does have a level when $x > x_{\mathrm{c}}$; to find the complete solution when the solution passes through the critical point, it is necessary to keep the momentum balance in integral form in order to properly conserve the continuity of the momentum across the critical point,

$$h_{i+1} = h_i + \frac{1}{\cos\theta} \left(\frac{\dot{V}^2}{g(\bar{A}_{i+\frac{1}{2}} \cdot \bar{A}_{i-\frac{1}{2}})} - \frac{\dot{V}^2}{g\bar{A}_{i+\frac{1}{2}}^2} + \Delta x \left(\sin\theta - S_{\mathrm{f}}\right)_{i+\frac{1}{2}} \right). \tag{16}$$

This implies that when going through the critical point, we can not use a "marching" method (e.g. Runge Kutta);

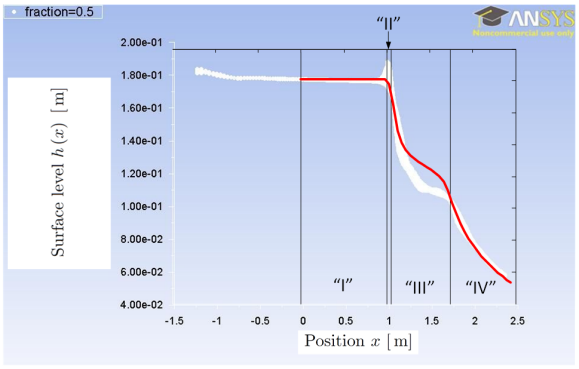

Fig. 3. Flow level profile in the Venturi flume with subcritical upstream flow condition; solution of SVE (solid red) overlaid over CFD solution. The location of Sections "I" – "IV" of the Venturi flume are indicated.

Table 1. Properties of Kaolin-based fluid Haldenwang (2003).

Properties	**Fluid**
Particle conc./vol. (%)	7.1
density, ρ [kg / m^3]	1118.5
yield stress, τ_0 [Pa]	10.551
fluid behavior index, K [Pa s^n]	0.834
fluid consistency index, $\frac{1}{\epsilon}$	0.387

instead the discretized model must use information from both downstream and upstream to the critical point. On the other hand, if the solution does not go through the critical point, the ODE formulation of (12) with a "marching" discretization algorithm can be used.

4. SIMULATION RESULTS

4.1 Case: water

We consider the case of $\theta = 0$, with water as fluid and flow rate 100.9 m^3 / h. CFD simulations are in excellent agreement with the flow rate-level tables specified by the flume manufacturer (maximum relative error of all simulations of 2%). Figure 3 shows the result of solving the SVE overlaid over the CFD solution in Malagalage et al. (2013).

In solving the SVE of the form (5) and (6), only the upstream boundary condition corresponding to the input flow rate of 100.9m^3 is specified. No downstream boundary is imposed since the flow is a free flow, and since it is revealed by CFD simulation that the flow passes through a critical point. The applied Manning roughness coefficient is 0.003. As can be seen, the result conforms to the CFD simulation result.

4.2 Case: drilling fluid

We change the Venturi flume slope to $\theta = 4°$, and consider a fluid characterized by the Herschel-Bulkley friction model with properties as given in Table 1.

Non-Newtonian fluid flow is often associated with high velocity to avoid fluid particle settling. This implies *supercritical* conditions and a corresponding level h_{s} which

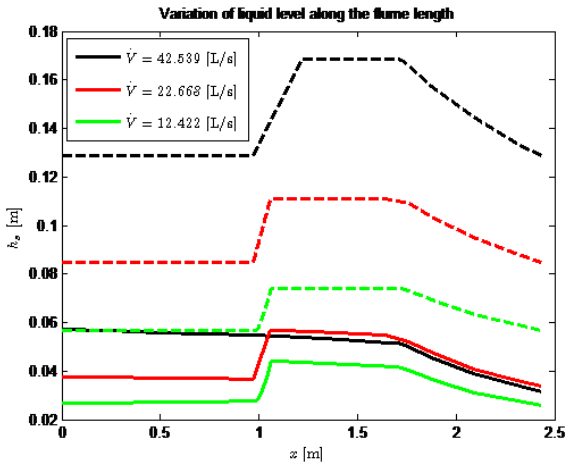

Fig. 4. Supercritical flow level profile (solid; above flume bed) in the Venturi flume with critical level (dashed); $W = 0.2\,\text{m}$.

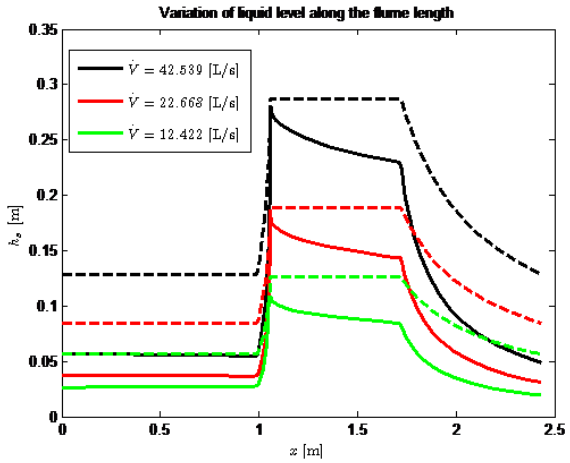

Fig. 5. Supercritical flow level profile (solid; above flume bed) in the Venturi flume with critical level (dashed); $W = 0.09\,\text{m}$.

is lower than the critical level; the solution is then found by solving (12). Here, we have used steady flow rates of $\{12.422, 22.668, 42.539\}$ [L/s]. The boundary conditions for the level is thus given upstream, at the inlet to Section "I" of Fig. 1 according to Haldenwang (2003). Figure 4 shows the resulting steady solutions.

From Fig. 4, we see that the Venturi flume does not lead to an increase in the level up to the critical level despite the hydraulic jump in the throat section (Section "III"), and it is not possible to find the flow rate from this design.

Next, we consider redesigning the Venturi flume by reducing the width of Section "III" to $W = 0.09$ [m]. The result is shown in Fig. 5.

In Fig. 5, it is seen that a hydraulic jump occurs in the channel throat section (Section "III") towards its exit, and this jump approaches the critical level.

4.3 Discussion

The results in the two cases indicate that the 1D steady state Saint Venant equation can predict a flow in a Venturi flume. Solving the SVE gives information about the flow rate and level distribution in the flume.

In the water case where the level goes through the critical point, the flume is divided into 50 discrete cells. Using a dynamic SVE, steady state is reached within 30 [s] taking some 1.5 [s] of computation time. In the drilling fluid case where the level reaches critical level due to hydraulic jump, the simulation of the steady SVE is executed with the MATLAB ode23 solver, which uses 10768 discretization points and takes 5.5 [s] to solve on a fairly standard PC.

CFD with results as in the backdrop of Fig. 3 gives much more information than SVE. However, to find these results takes in the order of 5 [h] of computer time. This time can be reduced somewhat if the initial transient from empty flume can be eliminated, but the computation time will still be high.

It has been indicated that by measuring the highest level in the throat section and assume this is the critical level, we can compute the flow rate using (14). However, the exact location where the critical level is reached, varies with the flow rate. Furthermore, for measurements, it is desirable with a steady, noise-free level. An alternative is thus to instead measure the level at uniform conditions, h_s^u, and compute $\dot{V}_\text{s}$ by equating $S_\text{fs}\left(h_\text{s}^\text{u}, \dot{V}_\text{s}\right) = \sin\theta$ similar to in (15), where we use the Herschel-Bulkley expression for friction slope. Thus

$$\dot{V}_\text{s} = \frac{\left(W h_\text{s}^\text{u}\right)^2}{W + 2h_\text{s}^\text{u}} \left[\left(\frac{W h_\text{s}^\text{u}}{W + 2h_\text{s}^\text{u}} \frac{\rho g}{\tau_0} \sin\theta \right)^{\epsilon+0.15} - 1 \right] \times \frac{(0.74 + 0.656\epsilon)}{(\epsilon+1)(\epsilon+2)} \left(\frac{\tau_0}{K}\right)^{\epsilon}. \tag{17}$$

Whether we use the Herschel-Bulkley model or some other friction model, the velocity expression will depend on the viscosity of the fluid.

Often, due to the short length of the flume, the uniform level is not reached, and (17) does not apply. Based on Bernoulli's equation, ISO (2013) develops an implicit expression for $\dot{V}_\text{s}$ as

$$\dot{V}_\text{s} = \left(\frac{2}{3}\right)^{\frac{3}{2}} \sqrt{\frac{g}{\beta}} \left(1 - \frac{0.006L}{W}\right) \left(1 - \frac{0.003L}{h_\text{s}}\right)^{\frac{3}{2}} \times \left(1 + \frac{\beta\left(\frac{\dot{V}_\text{s}}{W}\right)^2}{2gh_\text{s}^3}\right)^{\frac{3}{2}} W h_\text{s}^{\frac{3}{2}} \tag{18}$$

where L and W relates to the length and width of the throat section, and β is a tuning factor to handle different viscosities. Level h_s is measured in the middle of the throat section.

Another alternatively is to use the fully dynamic SVE, and combine the model with multiple level measurements in a state estimation scheme.

5. CONCLUSIONS

In this paper, CFD simulations of water flow in a zero slope Venturi flume have given excellent agreement with experimental results in the literature. Next, a simplified 1D model based on the Saint Venant Equations (SVE) has been analyzed, and found to give good agreement with the CFD model; better agreement is expected with improved tuning of boundary conditions for the SVE model. The SVE model has been used to simulate the case of drilling fluid flow in the same Venturi flume, with a 4° slope of the flume. Because low flow rate may lead to particle settling for drilling fluid, a high flow rate study is carried out. The study indicates that little information about the flow rate can be found using the nominal width of the Venturi flume. However, by narrowing the throat section of the flume, a significant jump in the level is achieved, and this level jump holds information about the flow rate.

Four possible methods for deriving the flow rate from the level jump are discussed in Section Discussion: (i) measuring the maximal level gives the flow rate independently of the fluid properties, (14), but the accurate level is complicated to measure, (ii) measuring the uniform level, the flow rate can be found if the fluid properties are known, (17) — but depends on a sufficiently long flume to reach uniform conditions, (iii) measuring some mid-way level can be used to derive the flow rate (18), but this method also depends on the fluid properties, and (iv) combining the transient SVE model in (5), (6) with multiple level measurements via state estimation is possible, but also depends on the fluid properties.

Future work will involve testing the various methods on a Venturi rig. Challenges for this future work include sensor set-up, the numerics of solving the SVE model, and efficient estimation algorithms.

REFERENCES

Aldrighetti, E. (2007). *Computational hydraulic techniques for the Saint Venant Equations in arbitrarily shaped geometry*. Ph.D. thesis, Universit'a degli Studi di Trento, Dipartimento di Matematica.

ANSYS-Inc (2011). *Ansys FLUENT Users's Guide*, 14 edition.

Bird, R.B., Stewart, W.E., and Lightfoot, E.N. (2002). *Transport Phenomena*. John Wiley & Sons, New York, second edition.

Chow, V.T. (1959). *Open-Channel Hydraulics*. McGraw-Hill.

Gupta, R.S. (2008). *Hydrology and Hydraulic Systems*. Waveland Press, third edition edition.

Haldenwang, R. (2003). *Flow of Non-Newtonian Fluids in Open Channels*. Ph.D. thesis, Cape Technikon, Cape Town, South Africa.

Hauge, S. and Øien, K. (2012). Deepwater horizon: Lessons learned for the norwegian petroleum industry with focus on technical aspects. *Chemical Engineering transactions*, 26, 621–626.

Hirt, C. and Nichols, B. (1981). Volume of fluid (vof) method for the dynamics of free boundaries. *Journal of Computational Physics*, 39(1), 201 – 225. doi: http://dx.doi.org/10.1016/0021-9991(81)90145-5.

ISO (2013). Flow measurement structures-rectangular, trapezoidal and u-shaped flumes. Technical Report ISO 4359, International Organization for Standardization, Switzerland.

Jin, M. and Fread, D. (1997). One-dimensional routing of mud/debris flows using nws fldwav model. In C. lung Chen (ed.), *Debris-Flow Hazards Mitigation: Mechanics, Prediction, and Assessment*, 687–696. ASCE, New York.

Malagalage, A., Berg, C., Agu, C., Chhantyal, K., and Mohammadi, F. (2013). Simulation of open channel flow for mass flow measurement. Msc project, Telemark University College.

Martinson, W.S. and Barton, P.I. (2002). Index and Characteristic Analysis of Linear PDAE Systems. *SIAM Journal on Scientific Computing*, 24(3), 905–923.

Smith, R., Chery, D., Jr., K.R., and Gwinn, W. (1981). Supercritical flow flumes for measuring sediment-laden flow. Technical Report Bulletin No. 1655, U.S. Department of Agriculture.

Versteeg, H.K. and Malalasekera, W. (2007). *An introduction to computational fluid dynamics : the finite volume method*. Pearson Education Ltd. cop., Harlow, England, New York.

Wilson, K. (1991). Flume design for homogeneous slurry flow. *Particulate Science and Technology*, 9, 149–159.